EUROfusion

WPDC-CPR(18) 20373

I Duran et al.

Steady-state magnetic diagnostic for ITER and beyond

Preprint of Paper to be submitted for publication in Proceeding of
30th Symposium on Fusion Technology (SOFT)

This work has been carried out within the framework of the EUROfusion Consortium and has received funding from the Euratom research and training programme 2014-2018 under grant agreement No 633053. The views and opinions expressed herein do not necessarily reflect those of the European Commission.

Status of steady-state magnetic diagnostic for ITER and outlook for possible materials of Hall sensors for DEMO

Ivan Ďuran[a], Slavomír Entler[a], Ondřej Grover[a], Inessa Bolshakova[b], Karel Výborný[c], Martin Kočan[d], Tomáš Jirman[e], George Vayakis[d]

[a]*Institute of Plasma Physics of the CAS, Prague, Czech Republic*
[b]*Magnetic Sensors Laboratory, Lviv Polytechnic National University, Lviv, Ukraine*
[c]*Institute of Physics of the CAS, Prague, Czech Republic*
[d]*ITER Organization, Route de Vinon-sur-Verdon, CS 90 046, 13067 St. Paul Lez Durance Cedex, France*
[e]*Imperial College, London, United Kingdom*

The ITER outer vessel steady state (OVSS) magnetic diagnostic employing bismuth Hall sensors is presently being manufactured. New results on understanding and analytical description of a rather complex dependence of bismuth Hall coefficient on magnetic field and temperature are presented. Both, dependence of bismuth Hall coefficient on temperature and magnetic field is captured by a single analytical function while the error of the fit is comparable to the maximum allowed error of the ITER OVSS diagnostic. Results of FISPACT simulation of indium transmutation under ITER OVSS like neutron fluence are presented. Indium is used within OVSS sensors to provide periodic in-situ recalibration of embedded thermocouples. It is demonstrated that additional impurities introduced by indium transmutation does not compromise precision of the ITER OVSS diagnostic. Finally, outlook for some DEMO perspective Hall sensing materials (InAs, Bi, BiCu, Bi, Sb, Au-nanofilms, Sb, and graphene) is given reviewing their properties in relation to the harsh environmental constrains posed their implementation on DEMO reactor.

Keywords: ITER, Hall sensors, steady state magnetic diagnostic

1. Introduction

Construction of ITER reactor and design work in the area of future next step fusion reactor called DEMO sparks increasing interest in the methods how to measure almost steady state magnetic field during long pulses of these devices. Outer Vessel Steady State (OVSS) magnetic sensors are integral part of the ITER magnetic diagnostic system [1]. The system is composed from 60 sensors in total grouped within 3 poloidal arrays each in the separate vacuum vessel sector, separated toroidally from each other by 120°. Sensors are mounted on the outer vacuum vessel skin fitting in the narrow gap between the vacuum vessel and the thermal shield. Each sensor unit measures tangential and normal component (with respect to the vacuum vessel) of the local magnetic field. The primary aim of this diagnostic system is to provide supplementary information on plasma current and the plasma-wall gaps. Original concept for this ITER diagnostic was based on Micro Electro-Mechanical System sensors (MEMS) however, this approach failed due to insufficient radiation hardness of the prototype MEMS sensors. Following that, Hall sensors based on bismuth sensitive layer were selected as the new concept for OVSS. Final design of the OVSS diagnostic for ITER, technology of sensors manufacturing and numerous tests validating their performance including neutron irradiation testing were conducted [2-7] resulting into demonstration that the selected approach to OVSS satisfies ITER requirements. Presently, the components of the OVSS diagnostic are at various stages of manufacturing process with the target date of installation on ITER in 2020.

In parallel, implementation of steady state magnetic sensors is contemplated also for future next step fusion reactor DEMO. Due to the inherent limitation of bismuth as a sensing material by its melting temperature of 271.7 °C and expected higher temperature of DEMO vacuum vessel, different materials have to be considered. Presently evaluated Hall sensing materials are golden nanofilms [8], bismuth reinforced by copper or antimony, pure antimony, InAs, and graphene.

This paper presents certain specific recent advancements in the field. Section 2 presents results of the recent evaluation of the bismuth Hall coefficient on magnetic field and temperature which is important for future calibration of the ITER OVSS sensors. Section 3 presents results of FISPACT simulation evaluating transmutation of indium under total neutron fluence expected at locations of ITER OVSS sensors. Indium capsule is used within ITER OVSS to periodically autocalibrate embedded thermocouple during its long term operation on ITER in order to ensure sufficient precision of temperature and consequently magnetic field measurement. Section 4 presents initial considerations on steady state magnetic diagnostic for DEMO and initial design of long term test of DEMO candidate Hall sensors within ITER port plug structure.

2. Dependence of Hall coefficient of the ITER Bismuth Hall sensors on the magnetic field and temperature

author's email: duran@ipp.cas.cz

The understanding of the dependence of the Hall resistance R_H on the magnetic field B and temperature T was further improved with respect to previous work [9]. Previously, the magnetic field and temperature dependencies were treated separately and did not yield a consistent function capturing both dependencies at once.

The new function $R_H(B,T)$ capturing both dependencies is derived for a 3-component electron gas mixture model where the i-th component has its own charge carrier density n_i and mobility μ_i. For simplicity and numerical tractability, the density includes the elementary charge as $n_i := n_i|e|$. At a given temperature the conductivity tensor of the i-th component is given by

$$\sigma_i = \frac{n_i \mu_i}{1+(\mu_i B)^2}\begin{pmatrix} 1 & \mu_i B \\ -\mu_i B & 1 \end{pmatrix} \quad (1)$$

and the transversal (off-diagonal) Hall resistivity ρ_{xy} is obtained from the inverse of the total conductivity tensor $\rho = \sigma^{-1} = (\sigma_1+\sigma_2+\sigma_3)^{-1}$. The improvement over the previous models lies in the assumption that each of the n_i and μ_i parameters has a specific temperature dependence.

In order to determine the temperature dependencies of $n_i(T)$ and $\mu_i(T)$ the Hall resistance mag. field dependence described by (1) with only 2 components was first fitted independently for each analyzed temperature in the set $\{27,67,97,127\}$ °C. The obtained dependencies are shown in Figure 1. Based on the observed trends the following assumptions on the temperature dependencies in the model were chosen.

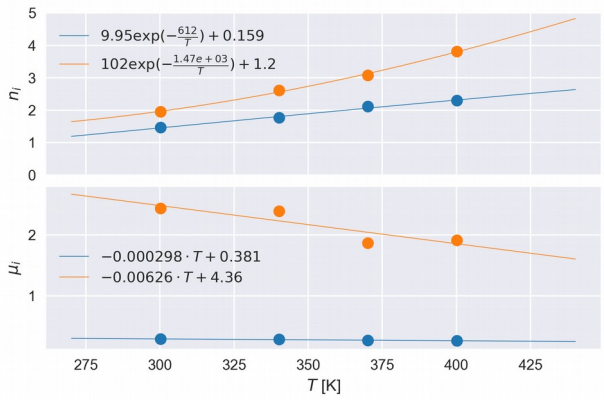

Fig. 1. The measured temperature dependence of the carrier density n_i and mobility μ_i of each component.

Each carrier density follows Boltzmann-like stastistics as

$$n_i = n_{0,i} + \frac{1}{Z}\exp\left(\frac{-E_{G,i}}{k_B T}\right) \quad (2)$$

where $n_{0,i}$ is the ground state density, $\frac{1}{Z}$ is the normalization by the partition function and $E_{G,i}$ is the gap energy. The fitted gap energy of the order ~ 0.1 eV is consistent with theoretical considerations. The mobility has a slight linear trend described as

$$\mu_i = \mu_{0,i} + pT \quad (3)$$

where $\mu_{0,i}$ is the average mobility and $p<0$ is small and reflects a slight decreasing trend of the mobility likely due to the increasing scattering on phonons at higher temperatures.

The full $R_H(B,T)$ dependence as a combination of (1), (2) and (3) for 3 components was then fitted to the data as a 2D function. The fitted parameters are summarized in Table 1 and the resulting 2D fit is shown in Figure 2.

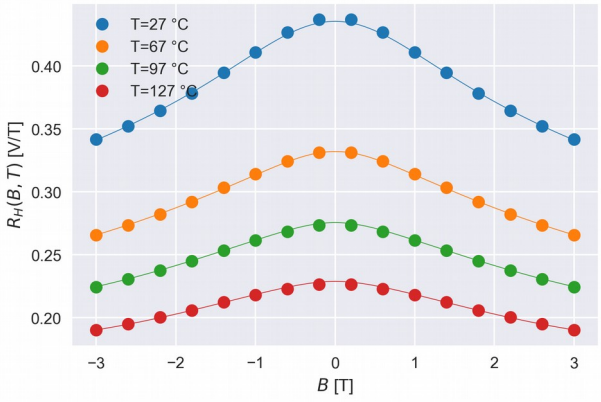

Fig. 2. Fit of the measured Hall resistance coefficient dependence $R_H(B,T)$ on the magnetic field and temperature.

Table 1 Fitted parameters in equations (2) and (3) for Figure 2

$n_{0,i}$	$E_{G,i}$ [eV]	$1/Z$	p	$\mu_{0,i}$
0.748	0.170	52.2	-0.0059	1.379
0.939	0.186	316.6	-0.0037	0.103
2.560	0.212	10.0	-0.0014	0.331

The corresponding maximum absolute error in the magnetic field measurement is about 3.4 mT, assuming linear error propagation. The fitting routine was specifically designed to minimize this value. Therefore, it is concluded that it is possible to fit a 2D $R_H(B,T)$ dependence with a maximum absolute error of the magnetic field of less than 4 mT.

3. FISPACT simulation of transmutation of indium capsules embedded within ITER OVSS for thermocouple in-situ recalibration

As mentioned in Section 2, Hall coefficient of bismuth features rather strong dependence on temperature. As a result, temperature of the Hall sensors will have to be precisely measured during their operation within ITER OVSS sensors. Type N nicrosil-nisil thermocouple will be embedded within each of the OVSS units in between the pair of Hall sensors. In order to fulfil the requirement on the steady state sensor magnetic field measurement accuracy, the temperature of the Hall sensor needs to be

author's email: duran@ipp.cas.cz

measured to 0.3 °C. In order to achieve this level of temperature measurement precision over the whole ITER life time, we embedded the thermocouple inside the e-beem welded cell filled by pure Indium. Melting point of pure natural indium is well established at T=156.598 °C [10]. Transient flat top in temperature evolution will be observed during periodic heating ramps of the ITER vacuum vessel up to 220 °C at Indium melting temperature due to phase transition. This phenomenon will serve as one point recalibration of each thermocouple periodically over the whole ITER lifetime.

However, the neutron radiation present during the ITER operation is going to activate Indium and cause transmutation. This process leading to increased impurity content can gradually have a critical impact on the Indium melting point. It has been shown that the impurities can have considerable impact on the melting point of Indium. [11]. Since this melting point is used for the sensor calibration it is crucial to quantify the amount of impurities introduced into indium due to the transmutation.

We used the FISPACT-II nuclear inventory code [12] to quantify indium transmutation when exposed to the maximum ITER life time neutron fluence of 3×10^{18} cm^{-2} expected at the locations of the OVSS sensors. Realistic neutron spectrum expected at these locations of ITER was used. Indium with natural composition of 95.8% of ^{115}In and 4.2% of ^{113}In was introduced into the simulation. Resulting material composition of the original natural indium after the FISPACT run is given within table 1 in terms of mass fraction. Because 5P clean natural indium with purity 99.999% will be used for OVSS sensors on ITER we present only isotopes with mass fraction higher than 10^{-6} within the table 2.

Table 2. FISPACT simulated material composition of the sample mass of natural indium after neutron irradiation by total fluence of 3×10^{18} cm^{-2} in terms of mass fraction.

Isotope	Mass fraction	Half life [s]
^{113}In	4.22×10^{-2}	stable
^{115}In	9.58×10^{-1}	1.39×10^{22}
^{116}Sn	6.54×10^{-5}	stable

FISPACT simulation revealed that we can expect slight deterioration of indium purity within OVSS sensors toward the end of ITER life time at level of up to 0.007% for sensors at the most neutron exposed locations. The only relevant impurity introduced by neutron irradiation is tin. The main interaction process involved is neutron capture in indium followed by decays. The leading neutron reaction chains of ^{115}In are:

$$¿+n \rightarrow {}^{116m}_{\square}¿ / {}^{116}_{\square}¿ \rightarrow {}^{116}_{\square}Sn + {}^{115}_{\square}e^{-¿}¿ \quad (4)$$

where half life of decay of ^{116m}In is 54 minutes and for ^{116}In it is 13 seconds. Similar processes work for ^{114}In isotope:

$$¿+n \rightarrow {}^{114m}_{\square}¿ / {}^{114}_{\square}¿ \rightarrow {}^{114}_{\square}Sn + {}^{113}_{\square}e^{-¿}¿ \quad (5)$$

where half life of decay of ^{114m}In is 72 seconds and for ^{114}In it is 50 days. Processes according to equation (4) dominate due to significantly higher concentration of ^{115}In in natural indium.

Melting temperature of In-Sn mixtures is widely studied because tin serves as a more nature friendly alternative to lead for vacuum compatible soldering. However, attention in these industrial applications is naturally not paid to In-Sn alloys with such microscopic content of tin as it is in our case. The most relevant results to our situation were found in [11] where the melting temperature of indium is studied as a function of its purity for 3 cases: 99.99%, 99.999%, and 99.9999% purity. In our case, OVSS sensors contain indium with purity 99.999% just after installation which will drop to 99.99% at the end of ITER lifetime. The maximum change of indium melting temperature $\Delta T=0.03$ °C can be expected in this case according to [11]. Because required accuracy of OVSS temperature measurement is 0.3 °C, we conclude that impact of indium transmutation on accuracy of the in-situ recalibration of ITER OVSS thermocouples is negligible.

4. Perspective of steady state magnetic field sensors for DEMO like environment

Precise determination of plasma - wall clearance during steady state operation of DEMO reactor is one of the critical challenges for design of the DEMO diagnostic set. One of the presently considered approaches to this task is employment of steady state magnetic sensors based on Hall effect. Although, the requirements set for steady state magnetic sensors (SSMS) on DEMO are in many aspect similar to those set for ITER OVSS, there are several differences which do not allow direct implementation of ITER OVSS sensors for DEMO. Primarily, the target life time neutron fluence for SSMD sensors on DEMO will be 2-4 orders of magnitude higher compared to ITER mainly due to much longer plasma operation time planned for DEMO. Secondarily, operation temperature of DEMO SSMS will be higher by at least 100 °C - 200 °C compared to the ITER value of approximately 100 °C. There are several possible locations of SSMS on DEMO from in-vessel (with most demanding environment), through mounting on outer side

author's email: duran@ipp.cas.cz

of vacuum vessel, till installation within far end of other auxiliary systems as neutral beams or other diagnostic systems requiring local magnetic field monitoring for their safe operation. As a result, different types of SSMS can be found optimum for each target application/location on DEMO. Presently evaluated concepts of SSMS are listed bellow.

4.1 Semiconductor sensors based on InAs

These semiconductor Hall sensors can be considered for lower neutron exposed locations of DEMO. Their radiation hardness was tested in the IBR-2 nuclear research reactor at the Joint Institute for Nuclear Research (JINR), in which the neutron energy spectrum is close enough to the neutron energy spectrum at the locations of the ex-vessel sensors in the ITER [13]. The sensitivity of the sensors remained stable up to total neutron fluence of 10^{17} cm^{-2} and decreased by only about 10% at neutron fluence of 10^{18} cm^{-2} depending on particular doping level of the sensitive layer. The neutron flux during irradiation was 10^{17} $cm^{-2}.s^{-1}$, and the irradiation temperature was 130 °C. The dependence of the signal of InAs semiconductor sensors on the magnetic field up to 14 T is linear in a wide temperature range [14].

On the basis of InAs semiconductor sensors, the magnetic measuring equipment was created, which was installed in 2009 in the JET tokamak and it is still in routine operation. The long-term stability of the sensors was evaluated by statistical processing of the data for the first 5 years of operation of the sensors encompassing over 8500 JET pulses and showed that the stability of the sensors sensitivities over the five-year period is within ±0.1% of the baseline data [15].

4.2 Metal Hall sensors based on Bi and BiCu/BiSb

Bismuth, is the metal (sometimes called semi-metal) with highest Hall coefficient among all metals thanks to its specific electron band structure. Bismuth Hall sensors developed and employed for ITER OVSS sensors [2-7] feature radiation stability of their sensitivity within a few percent up to the total neutron fluence of 8×10^{18} cm^{-2} as demonstrated during irradiation experiment on LVR-15 fission reactor. Nonlinear dependence of bismuth Hall coefficient on temperature and magnetic field (see Sec. 2) [9] has to be handled by calibration. Main limitation with respect to the use of these sensors for DEMO reactor is relatively low melting temperature of bismuth at 271.5 °C. By adding a small impurity of copper or antimony at the order of a few percent we managed to operate bismuth Hall sensors even significantly above bismuth melting temperature but we observed sharp drop of sensitivity for temperatures above 271.5 °C which makes use of such sensors impractical [16]. The reason is massive injection of free charge carriers after breakdown of bismuth band gap structure due to local melting and consequent drop of sensitivity.

4.3 Metal sensors based on Au-nanofilms

Recently, sensors based on gold nanofilms of thickness (50-70) nm and the size of the sensitive area (0.2×0.2) mm^2 were created with ambition to provide solution for the DEMO measurement locations with highest neutron loads. Gold is widely used in microelectronics, it is known that gold elements have the least fluctuations in electrical conductivity, which are the cause of noise of 1/f type [17]. The testing of gold sensors in neural fluxes was carried out in IBR-2 nuclear reactor using on-line measurements during prolonged irradiation for 1842 hours to achieve a DEMO-relevant fluence of 10^{20} cm^{-2}. Throughout the whole range of studied fluences up to the highest 10^{20} cm^{-2}, the main parameter of gold sensors - sensitivity to the magnetic field, remains stable within the measurement error [8]. The absence of degradation of gold sensors at such high fluences makes it possible to hope for the possibility of operability of these sensors at even higher radiation doses. The results of the measurements confirm the promise of metal Hall sensors based on gold nanofilms for use in magnetic measurement tasks under high neutron fluences.

4.4 Antimony Hall sensors

Hall sensors based on pure antimony layer were also recently investigated as the higher temperature resistant alternative to bismuth Hall sensors. First results summarized in [16] show that Hall sensors prepared according to ITER OVSS sensors design [7] just with 1 μm thick layer of antimony instead of bismuth, feature sensitivity around 25 mV/(A.T) at room temperature which is intermediate value between pure bismuth sensors and golden nano-layer sensors. Operation of the sensors up to 500 °C was demonstrated. Linear dependence of Hall voltage on temperature was measured in the DEMO relevant range ~ 190 °C – 350 °C. Hall voltage is also a linear function of magnetic field in the investigated range ±14 T. Initial neutron irradiation tests of the pure antimony Hall sensors are under preparation.

4.5 Graphene Hall sensors

One of the promising materials for Hall sensors, able to work in the severe radiation environment is a new electronics material of graphene. Theoretical studies predict the high radiation resistance of graphene and its amazing ability to self-heal defects [18]. An evaluation of the effect of irradiation by neutrons on the structure of graphene was carried out by comparing the Raman spectra before and after irradiation with neutrons to neutron fluence of 4.5×10^{15} cm^{-2}. Typical Raman spectra before and after irradiation of graphene with graphene-specific lines D, G and 2D are shown in Fig. 3. From Fig. 3 it is seen that the D-line of the spectrum after irradiation remains the same as before the irradiation. From this we can conclude that neutron irradiation does not lead to the damage of the structure of graphene.

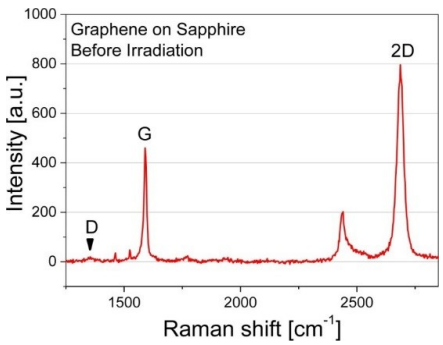

author's email: duran@ipp.cas.cz

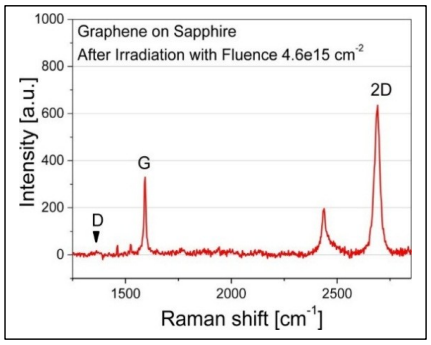

Fig. 3. Raman spectra of graphene before (top) and after (bottom) neutron irradiation.

5. Summary

We present the new solid state physics based approach to describing complex dependence of ITER bismuth OVSS sensors sensitivity on temperature and magnetic field. Measured data were fitted by analytical 2D formula while the precision of the fit is within the maximum ITER OVSS error boundaries. FISPACT simulation of indium transmutation demonstrated that additional impurities introduced by transmutation does not compromise precision of ITER OVSS periodic in-situ recalibration of embedded thermocouples and as a result does not compromise long term precision of the OVSS diagnostic. The last part of the paper presents outlook for some Hall sensor materials suitable for application in even more demanding radiation and thermal environment of the future DEMO reactor.

Acknowledgments

This work has been carried out within the framework of the EUROfusion Consortium and has received funding from the Euratom research and training programme 2014-2018 under grant agreement No 633053 co-funded by MEYS project number 8D15001. The experiment was performed in the Materials Growth and Measurement Laboratory MGML (http://mgml.eu). The views and opinions expressed herein do not necessarily reflect those of the ITER Organization and the European Commission.

References

[1] G. Vayakis et al, Development of the ITER magnetic diagnostic set and specification, Rev. Sci. Instr. 83 (2012) 10D712.

[2] M. Kocan et al., Final design of the ITER outer vessel steady-state magnetic sensors, Fus. Eng. Des. 123 (2017) 936-939.

[3] I. Duran et al., Development of Bismuth Hall sensors for ITER steady state magnetic diagnostics, Fus. Eng. Des 123 (2017) 690-694.

[4] I. Duran et al., High magnetic field test of Bismuth Hall sensors for ITER steady state magnetic diagnostic, Rev. Sci. Instr. 87 (2016) 11D446.

[5] S. Entler et al., Signal conditioning and processing for metallic Hall sensors, Fus. Eng. Des 123 (2017) 783-786.

[6] S. Entler et al., Recent improvement of the Design of the ITER Steady-State Magnetic Sensors, IEEE Trans. on Plasma Science 46 (2018) 1276-1280.

[7] M. Kocan et al., Steady state magnetic sensors for ITER and beyond: development and final design, Rev. Sci. Instr. (2018) in press.

[8] I. Bolshakova et al., Metal Hall sensors for the new generation fusion reactors of DEMO scale, Nucl. Fus. 57 (2017) 116042

[9] S. Entler et al., High magnetic field and temperature test of the ITER outer vessel steady-state magnetic field Hall sensors at ITER relevant temperatures, Rev. Sci. Instr. 89 (2018) 10J112.

[10] G.F. Strouse, Special Publication (NIST SP) – 260-132.

[11] J. Ancsin, Melting Curves and Heat of Fusion of Indium. Metrologia 21 (1985) 7-9.

[12] J.-Ch. Sublet et al., FISPACT-II: An Advanced Simulation System for Activation, Transmutation and Material Modelling, Nuclear Data Sheets 139 (2017) 77-137.

[13] M. Bulavin et al., Irradiation facility at the IBR-2 reactor for investigation of material radiation hardness, Nucl. Instrum. Methods Phys. Res. B 343 (2015) 26–9.

[14] I.S. Vasilevskii et al., Investigation of semiconducting materials for magnetic field sensors in strong magnetic fields under cryogenic temperatures, Book of Abstr. of 7th International Scientific and Practical Conference on the physics and technology of nanoheterostructural microwave electronics (May 25, 2016) P. 139–140.

[15] I. Bolshakova et al., Magnetic measuring instrumentation with radiation-resistant Hall sensors for fusion reactors: experience of testing at JET IEEE Trans. Nucl. Sci. 59 (2012) 1224–31.

[16] S. Entler et al., Prospects for the steady-state magnetic diagnostic based on antimony Hall sensors for future fusion power reactors, these proceedings of SOFT 2018.

[17] Hoge F.N., 1/f noise, Physica B 83 (1976) 14–23.

[18] J. Chen et al., Self healing of defected graphene, Appl. Phys. Lett. 102 (2013) 103107.

author's email: duran@ipp.cas.cz